University of Tehran Press

Pollution

https://jpoll.ut.ac.ir/

Print ISSN: 2383-451X
Online ISSN: 2383-4501

Quartz Mineral as new Sorbent for Hg(II) Removal from Aqueous Solution: Adsorption Kinetics and Isotherm

Nouar Sofiane Labidi[1*] | Boukoffa Mechati[2]

1. Department of Matter Sciences, Faculty of Sciences and Technology, University of Tamanrasset 11000, Tamanghasset, Algeria
2. Department of Geology, Faculty of Sciences and Technology, University of Tamanrasset 11000, Tamanrasset, Algeria

Article Info

Article type:
Research Article

Article history:
Received: 20 June 2022
Revised: 17 Nov 2022
Accepted: 02 Jan 2023

Keywords:
SiO_2
Hg(II)
Wastewater
Kinetic
Physisorption

ABSTRACT

Natural quartz mineral was examined as a new sorbent for Hg(II) removal from synthetic wastewater systems. Batch adsorption experiments of Hg(II) onto quartz mineral were conducted under various conditions such as solution pH, sorbent dosage, contact time, initial Hg(II) concentration. Adsorption experiments results of Hg(II) by quartz mineral showed good achievement after 180 min with 1.0 g/L sorbent mass at pH of 2.0, agitation speed of 200 rpm and a temperature of 25°C. Moreover, the Hg(II) concentration was directly related to increases the adsorption capacity, the maximum Hg(II) uptake by quartz sample was 16.52 mg/g for 80 mg/L (C0 (Hg(II)]. Langmuir isotherm and pseudo-second-order kinetics (R2 > 0.99) were found to be the most appropriate models to describe the adsorption of Hg(II) by quartz mineral. The intra-particle diffusion model and the calculated Dubinin–Radushkevich adsorption energy (E_{ads} = 0.78 $kJmol^{-1}$), confirms a physisorption adsorption reaction occurring in three stages.

Cite this article: Labidi, N. S. & Mechati, B. B. (2023). Quartz Mineral as new Sorbent for Hg(II) Removal from Aqueous Solution: Adsorption Kinetics and Isotherm. *Pollution* , 9 (2), 1-14.
http//doi.org/10.22059/POLL.2022.344756.1514

 Publisher: University of Tehran Press.
DOI: http//doi.org/10.22059/POLL.2022.344756.1514

INTRODUCTION

Heavy metal contamination is a major problem due to the potentially harmful impacts of these chemicals in the environment. They can be introduced into the environment by natural sources and anthropogenic activities. Natural sources of mercury include volcanic action, weathering of mercuriferrous rocks, degassing from surface water, biogenic emissions, and forest fires (Volesky,1994), while anthropogenic activities, such as chemical manufacturing, metallurgical industries and artisanal gold mining, paper industry, pharmaceuticals, seed dressings, fungicides, dental preparations, thermometers, paints, fluorescent and ultraviolet lamps and fuel consumption (Volesky,1994; Tuzen et al., 2009).

Mercury is a very hazardous heavy metal that stays in the environment long after the cause of poisoning has been eradicated (Kang et al., 2020; Di Natale et al., 2005). Because of its high toxicity, World Health Organization (WHO) limited the maximum allowable limits of Hg(II) to 1.0 μg/L and 5.0 μg/L in drinking and wastewater, respectively (Al-Ghouti et al., 2019; Al-Yaari and Saleh, 2022). Hence, the removal of mercury from contaminated water is desirable.

*Corresponding Author Email: *labidi19722004@yahoo.fr*

Several approaches, involving precipitation, ion exchange, filtration, membrane technology, extraction technology, electrochemical processes, and adsorption, have been used to remediate heavy metals from wastewater (Olugbenga et al., 2014). Adsorption is a successful method for removing dyes from wastewater in terms of efficiency and cost when compared to other conventional remediation methodologies (Labidi et al., 2022).

In recent years, a wide range of materials has been demonstrated to be effective for Hg (II) removal from wastewater such as:pozzolana (Di Natale et al., 2006), MoS_4-LDH (Ma et al., 2017), silica (Kosak et al., 2015; Wang et al., 2018), functionalized Fe_3O_4 (Jianjian et al., 2020), kaolin (Yilmaz et al., 2017), zeolite (Rostami et al., 2018; Fang et al., 2018), coal (Liangyan et al., 2020), L-cystine/LDHs (Bingbing et al., 2020), hydroxylapatite (Kim & Lee, 2014), bentonite (Wang et al., 2011), chitosan (Bhatt et al., 2018) and pyrite (Yucheng et al., 2020). Since commercially available synthetic materials are expensive, exhibit slow kinetics with a limited adsorption capacity and difficult to regenerate, looking for additional new natural low-cost materials is needed.

In this paper natural quartz mineral was chosen as a new adsorbent for Hg(II) species in synthetic wastewater. Because of the porous texture, mechanical stability, good-quality surface, non toxic and natural character, geological abundance in Algeria (Tamanghasset south region), the quartz mineral used in this study is cheap and presents an economic advantage as natural low-cost adsorbent.

The present study reports the application of Algerian white quartz mineral as new natural sorbent for the removal by adsorption of Hg(II) species from aqueous solutions. The main parameters affecting the adsorption process such as sorbent dose, solution pH, temperature initial sorbate concentration and contact times, were investigated. The isotherm constants for the Langmuir, Freundlich, Temkin and Dubinin–Radushkevich (D-R) isotherms have been calculated using the linear models. Kinetics study was carried out using the pseudo-first-order (PFO), pseudo-second-order (PSO) and intra particle diffusion (IPD) models.

MATERIAL AND METHODS

Materials and reagents

A mining company provided the quartz material (Figure 1). The samples were washed in distilled water, dried at 110°C for 24 hours, then crushed in a ceramic ball mill and sieved using ASTM standard sieves to get particles size ranging from 100-80µm . A 50 g of quartz was sieved for 10 minutes to determine the particle size distribution of the sample used for adsorption experiments (Table 1).

Stock solution of mercuric ions (1000 mg/L) was prepared by dissolving suitable quantity of

Fig. 1. Quartz mineral (**left**) and the powder fraction (100-80µm) (**right**)

Table 1. Particles size distribution of quartz mineral.

Size range	weight (%)
> 100µm	3.87
100-80µm	24.00
80-60µm	19.95
60-40µm	19.44
40-20µm	18.53
20-10µm	9.71
< 10µm	4.50

$Hg(NO_3)_2 \cdot H_2O$ (Fluka Chemika) in double-distilled water. Working standards were prepared by diluting different volumes of the stock solution using double-distilled water to obtain the desired concentration. The solution pH was adjusted by adding a few drops of 0.1 M NaOH and HNO_3. The amount of Hg(II) species in the solution was determined from an established calibration curves using Flame Atomic Absorption Spectrophotometer (PYE *Unicam SP9*) at a wavelength λ of 253.7 nm (Bhatt et al., 2018; Al-Ghouti et al., 2019; Al-Yaari and Saleh, 2022).

Materials characterization

The chemical composition of the quartz mineral is given by XPS (Cameca SX-50). The morphology of quartz was collected on a Scanner Vega3 scanning electron microscope equipped with an energy dispersive X-ray spectrometer (SEM/ EDS) with an acceleration beam of 15 kV. A BRUKER AXS with generator (10 kV) was employed as the X-ray diffractometer. The Cu-$K\alpha_1$ monochromatic radiation (λ= 1.5406Å) was used to collect the diffractogram. The FTIR measurement was done with a JASCO 460 spectrometer that came with OMNIC software and has a wavelength range of 400/cm to 4000/cm with a resolution of 4 cm^{-1}. The surface area (m^2/g) was measured by Sear's method using the following equation: S (m^2/g) = 32× (V_b-V_a) - 25, where V_b and V_a are the volumes of the basic and acidic solutions, respectively (Sears, 1956).

Electrokinetic measurements

The electrokinetic characteristics were measured using a Laser Zee Meter (Pen Kem Inc), at a voltage of 100 V and a temperature of 25°C. Quartz particles were suspended in distilled water containing 10^{-3} M KNO_3 and agitated for 2 hours, the pH was adjusted using 0.1M HNO_3 and NaOH solutions (Purohit et al., 2006). OHAUS (Starter 3100) pH meter was used to determine the pH before and after the zeta potential experiments.

Adsorption experiments

To assess the impact of sorbent quantity on Hg(II) adsorption at 25°C, variable amounts of sorbent from 0.12 to 1.0 g/L were used. The experimental variables are kept constant, a contact time of 180 minutes, Hg(II) concentration of 100 mg/L, the suspensions pH of 2.0 and an agitation speed of 200 rpm.

The removal effectiveness of Hg(II) ions by quartz mineral in a pH range of 2.0-12.0 was examined using 1.0 g/L of quartz at 25°C with an initial Hg(II) concentration of 50 mg/L, agitation speed at 200 rpm and a contact time of 180 minutes. The pH of the solution was adjusted by (0.1M) HNO_3 and NaOH solutions.

Batch adsorption of mercuric ions onto quartz surface was carried out at 25°C, pH = 2 and an agitation at 200 rpm. Adsorbent dose of 1.0 g/L was added to 100mL Hg(II) solutions of different concentrations from 20 to 500 mg/L. After an equilibrium time of 180 min, the Hg(II) ions in solution were separated from the adsorbent by centrifugation at 2000 rpm for 15 minutes. The

amounts of Hg(II) species were determined by atomic absorption spectroscopy (PYE *Unicam SP9*). The adsorption capacity (q_e) and the removal efficiency (R %) of quartz sorbent for Hg(II) were calculated by equations (eq.1) and (eq.2) (Ho et al., 2000):

$$q_e = \frac{(C_0 - C_e)V}{m} \qquad (eq.1)$$

$$R\% = \left[\frac{C_0 - C_e}{C_0}\right] \times 100 \qquad (eq.2)$$

Where C_i and C_e denote the initial and equilibrium concentrations (mg/L), m is the mass of quartz (g), and V denotes the solution volume (L).

Kinetics investigations were conducted with an Hg(II) concentration of 500 mg/L. A 100 mL mercury solution is mixed with 1.0 g/L g of adsorbent that are 100-80µm in size. The suspensions are stirred at 200 rpm with an agitation time from 5 to 280 minutes at 25° C and pH = 2.0. At the end of adsorption the Hg(II) ions were separated from the suspension by centrifugation at 2000 rpm for 15 minutes and analysed for the residual Hg(II).

RESULTS AND DISCUSSION

The chemical composition of the quartz mineral is given by XPS (Cameca SX-50). It contained about 99.13% SiO_2, 0.34% CaO, 0.31% MgO and 0.22 % Fe_2O_3.The surface area of quartz measured by Sear's approach was 0.60 m^2/g, which agrees well with that found using the BET methods (Tabrizy et al., 2011), they found that quartz has a specific surface area of 0.62 m^2/g for N_2, 0.67 m^2/g for Kr and 0.65 m^2/g for H_2O. Figure 2 shows the X-ray diffraction pattern of quartz. The usual characteristic peaks of the quartz sample are around 2θ = 20.88°, 2θ = 26.78° and, 2θ = 50.01°and 2θ = 55.5°, 2θ = 60.0° and 2θ = 68.7° which correspond to the miller indices:

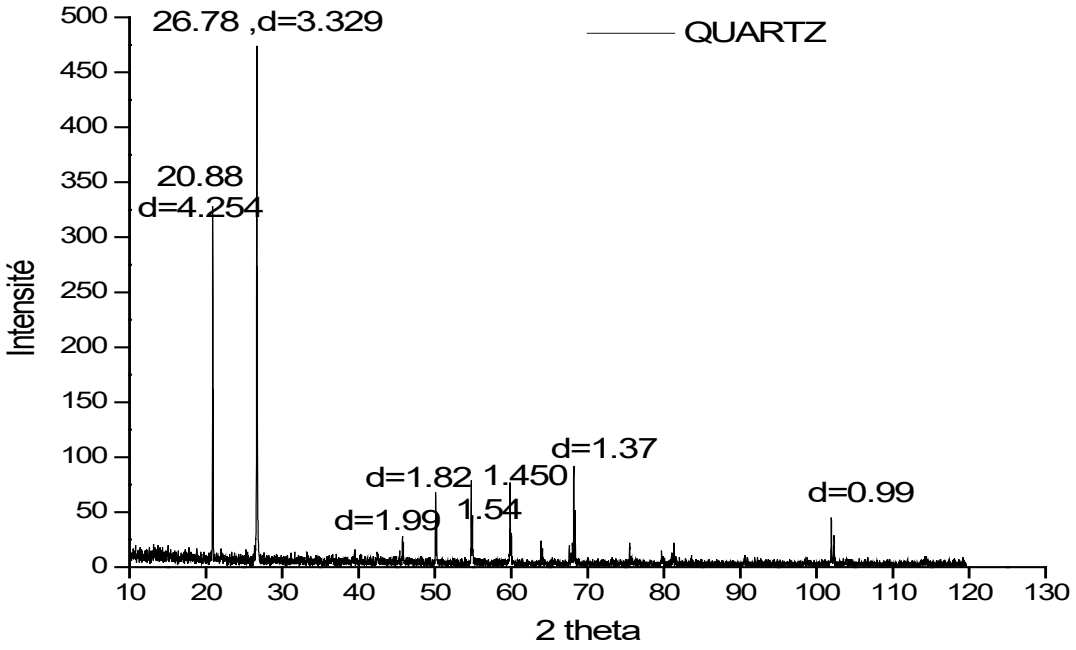

Fig. 2. X-ray diffraction pattern of quartz mineral.

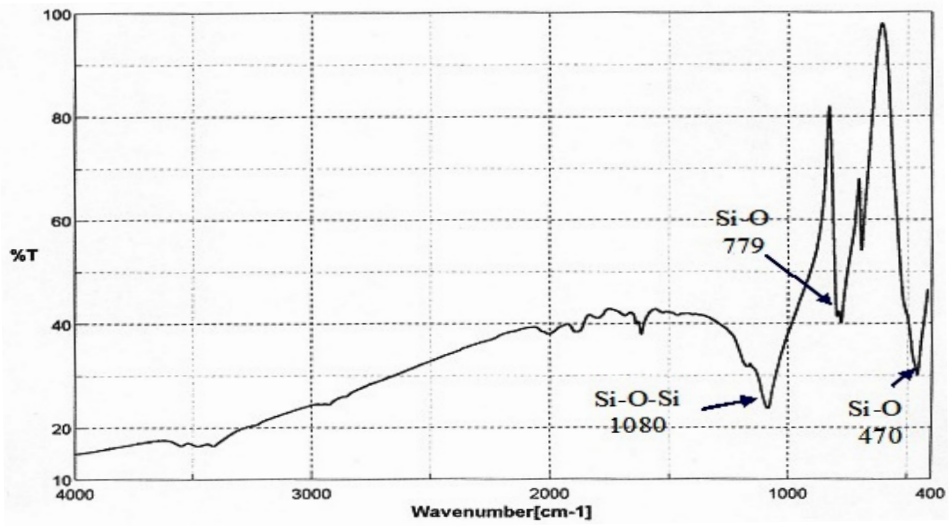

Fig. 3. FTIR Spectrum of quartz mineral.

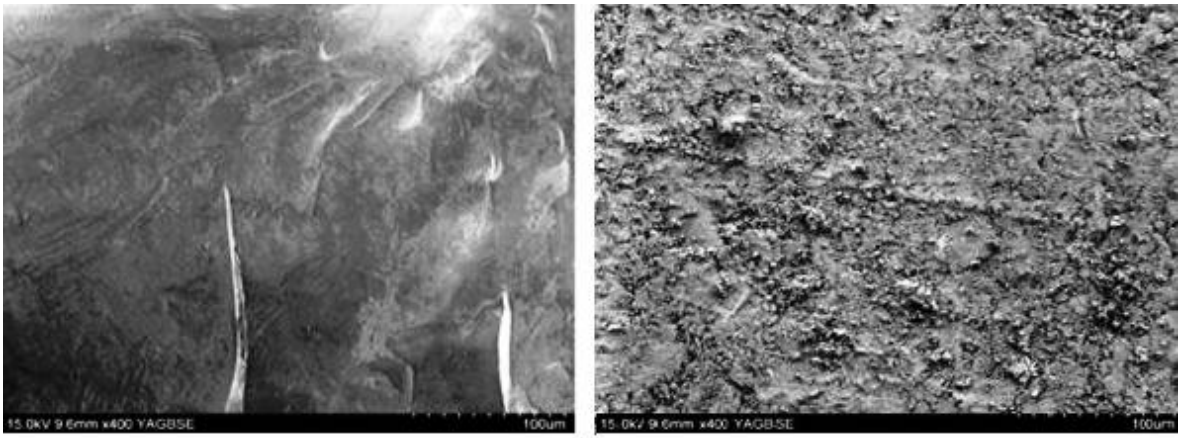

Fig. 4. SEM image of the quartz surface (before and after grinding)

(110), (011), (112), (013), (211) and (031), by comparison with the standard JCPDS No. 5-0490 (Nadhiraet al., 2018). The quartz X-ray peaks are identical to those of pure quartz (Levien et al., 1980).

The FTIR spectrum of quartz is shown in Figure 3. The most important absorption peaks are in the range 470 to 1100 cm^{-1}, which corresponds to the asymmetric stretching of Si–O–Si groups at 1080 cm^{-1} and the symmetric stretching at 779 cm^{-1}, accordingly. However, at 470 cm^{-1} and 520 cm^{-1}, respectively, the asymmetric and symmetric Si–O bending modes are seen. The absorption peaks located at 3450 cm^{-1} and 1630 cm^{-1} correspond to the hydroxyl group OH and the deformation of the H_2O molecules respectively (Saikia et al., 2008).

The surface morphology of the quartz mineral before and after grinding is shown in Figure 4. The surface of SiO_2 before grinding appears compact and heterogeneous through different shape of undulations and cuts. However, after grinding a hilly surface with an important evolution of the roughness in the perimeter of the inspected surface is observed.

The knowledge of the chemical behavior of the metal ion and the sorbent material may help to achieve the finest results in the sorption process. Figure 5 illustrates the zeta potential of quartz in KNO_3 electrolyte solution as function of pH. Quartz's isoelectric point (I.E.P) was

determined to be at pH close to 1.8. Below this pH, the surface is negatively charged, and the strength of the charge rises with increasing the pH value. At pH = 7.0 the zeta potential is -17.84 mV. However, at pH = 10.0, the zeta potential is more negative and reach -19.23 mV.

The effect of sorbent dose is presented in Figure 6.As shown with an adsorbent mass ranging from 0.12 to 1.0 g/L, the percent removed of Hg(II) increases from the minimum of 38.45% to the maximum of 99.60 %, respectively. The maximum removal capacity (99.60 %) was reached for a quartz dose of 1.0 g/L, at which the adsorption active sites were sufficient for complete adsorption (≈100%). This can be attributed to the increase in the quartz surface area and the available active sites (Al-Yaari and Saleh, 2022). Therefore, for further experimental setup, 1.0 g/L adsorbent dosage was used. Similar results have proven that an increase in the dosage of adsorbent at a constant pH and adsorbate concentration has positive effect on the removal of for heavy metals pollutants from wastewater (Zhang et al., 2011; Fang et al., 2018; Hadi et al., 2015).

The influence of pH on mercuric ion removal at various pH levels ranging from 2.0 to 12.0 is exposed in Figure 7. It was observed that Hg(II) removal increased with increasing solution pH from 2.0 to 6.0, then decreased as the solution pH > 6. The highest and the lowest retention capacities of 3.32 mg/g and 1.94 mg/g were observed for pH values close to 6.0 and

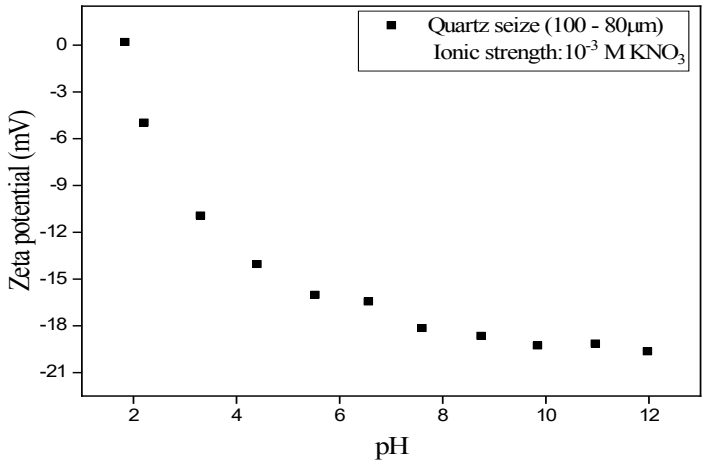

Fig. 5. Zeta potential of quartz as function of pH in KNO_3 electrolyte solution ([KNO_3] = 10^{-3} M at 25 °C).

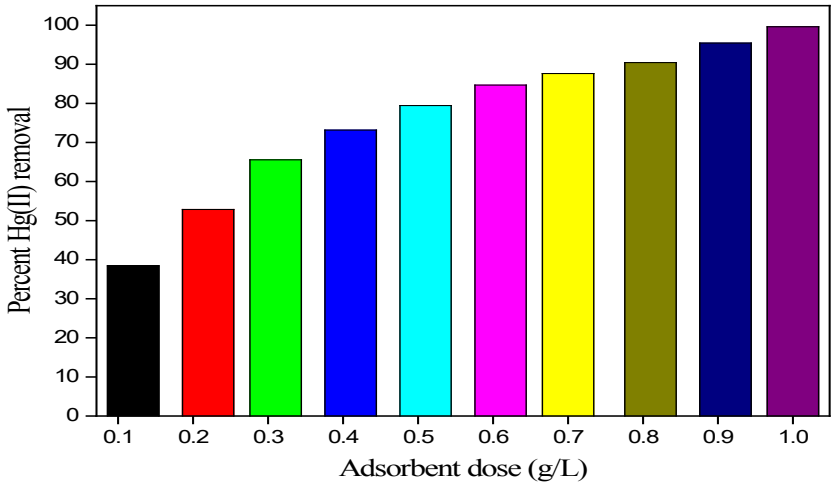

Fig. 6. Effect of sorbent mass on Hg(II) removal (pH= 2.0, [Hg(II)] = 100 mg/L and T = 25°C contact time = 180 min ; agitation speed = 200 rpm).

2.0, respectively. The higher removal amount obtained at pH > 2 is due to metal hydrolysis and the onset precipitation (Marin et al., 2020).The interaction between Hg(II) species with the quartz surface as a function of pH can be explained across the chemistry of mercury species and the quartz characteristics. The zeta potential of quartz in KNO_3 electrolyte solution at various pH ranges from 2.0 to 12.0 (see Fig.5), reveals that the quartz surface is negatively charged between 1.8 < pH £ 12. According to the Hg(II) speciation diagram (Powell et al., 2005), at very low pH(pH £ 2), Hg(II) are the dominant species for sorption in most aqueous solutions. The metal hydrolysis reactions and the onset precipitation of Hg(II) are significant at pH > 2 . The high removal capacity over the pH range from 3.0 to 6.0 is essentially due to the strong Lewis acidic nature, the dominant hydrolysis Hg(II) species formed $HgOH^+$ and $Hg(OH)_{2(aq)}$ (log $K_{1,OH}$ = -3.5 and log $K_{2,OH}$ = - 4.0) (Babic et al., 2002). In this pH range the quartz becomes more attractive to the hydrolyzed species, thus increasing sorption. At pH from 6.5 to 12.0, The decrease in the metal removal as increasing the solution pH can be explained by the decrease in the hydrolyzed species and the formation of other major Hg(II) species such as $Hg_2(OH)_2^{2+}$ and trimer $Hg(OH)_3^-$(log$K_{3,OH}$ = -14.8) (Babic et al., 2002).

From the speciation study on the Hg(II) ions in aqueous phase (Powell et al., 2005; Babic et al., 2002), with particular reference to its hydrolysis in the pH range from 2.0 to 6.0, Hg(II) is

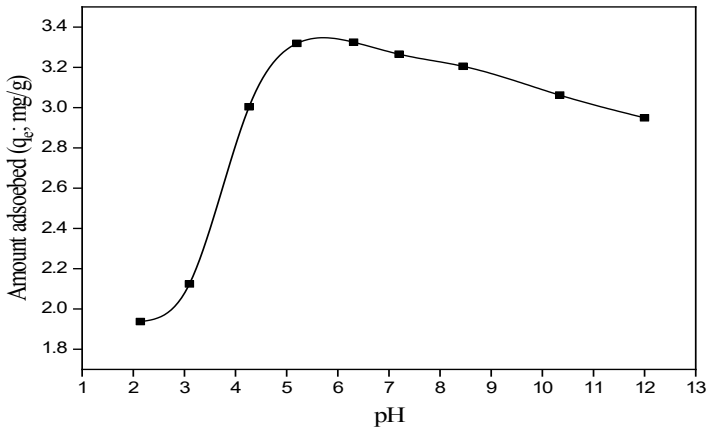

Fig. 7. Effect of solution pH on Hg(II) uptake (T = 25 °C; adsorbent dose = 1.0 g/L; [Hg(II)] = 50 mg/L and agitation speed = 200 rpm).

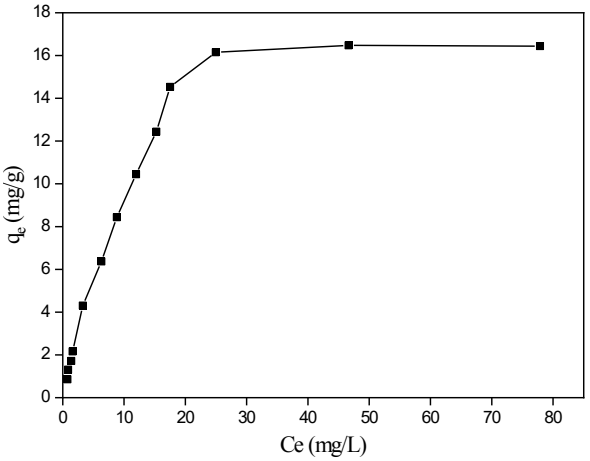

Fig. 8. Adsorption isotherm of Hg(II) onto quartz ([Hg(II)] = 20-500 mg/L; adsorbent dose = 1.0 g/L, T=25 °C, pH = 2.0 and agitation speed = 200 rpm).

the dominant form in aqueous solutions only at pH £ 2. For this reason the subsequent studies were conducted at pH 2.0.

Batch adsorption of mercuric ions onto quartz surface was carried out at 25°C and pH = 2, by adding 1.0 g/L of quartz into 100 mL of Hg(II) at different concentration from 20 to 500 mg/L. Figure 8 illustrates the adsorption isotherm of Hg(II) onto quartz. The isotherm is of the Langmuir type, as demonstrated (L). With increasing concentrations, the adsorbed quantity of Hg (II) increases. The highest uptake achieved by quartz mineral is 16.52 mg/g.

The adsorption isotherms were used to describe the adsorption mechanism of Hg(II) ions onto quartz surface. Three models including Langmuir (eq.3), Freundlich (eq.4) and temkin (eq.5) isotherms were used to assess the equilibrium adsorption data (Hui et al., 2019; Al-Ghoutiet al., 2019).

$$\frac{1}{q_e} = \frac{1}{q_m} + \left(\frac{1}{q_m K_L}\right) \times \frac{1}{C_e} \qquad (eq.3)$$

$$Log\left(q_e\right) = LogK_F + \left(\frac{1}{n}\right) Log(C_e) \qquad (eq.4)$$

$$q_e = B\,LnA + B\,Ln(C_e) \qquad (eq.5)$$

Where q_e and C_e are the adsorbed amount (mg/g) and equilibrium concentration (mg/L) of Hg(II), respectively; q_m is the maximum adsorbed amount ($mg.g^{-1}$) and K_L (L/mg) is the Langmuir constant. K_F and n are Freundlich's uptake and intensity factors. B is associated to the heat of sorption, and A(L/mg) is the equilibrium binding constant. The Langmuir, Freundlich, and Temkin isotherm constants as well as the coefficients of determination were obtained using the linear method which consisted of plotting 1/qe versus $1/C_e$, $\log(q_e)$ versus $\log(C_e)$, and q_e versus $\ln(C_e)$, respectively (Table 2).

The obtained results are presented in Figure.9 and listed in Table 2. It was observed that the value of correlation coefficient (R^2) for Langmuir model was higher than those of other three models. The linear Langmuir isotherm model produces a straight line with a correlation coefficient $R^2 = 0.995$ (Fig.9a), suggesting a monolayer uptake onto the quartz surface (Di Natale et al., 2006; Fang et al., 2018). The calculated sorption capacity (q_m) is equal to 33.29 mg/g,

Table 2. Isotherms parameters for the adsorption of Hg(II) onto quartz.

Langmuir constants		
$q_{e,cal}$ (mg/g)	K_L(L/mg)	R^2
33.26	0.023	0.995
Freundlich constants		
K_F(L/g mg)	1/n	R^2
0.74	0.82	0.987
Temkin constants		
B	A (L/mg)	R^2
7.66	0.10	0.976
Dubinin–Radushkevich		
q_s(mol/g)	β(mol^2/kJ^2)	R^2 E(kJ/mol)
1.19×10^{-3}	-0.828	0.987 0.78

the Langmuir constant (K_L= 0.023 (L/mg)) and the separation factor (R_L = 0.10) point out that adsorption is favorable. The positive B value calculated from the Temkin model indicated an exothermic adsorption process (Bahtt et al., 2018). Similar result was obtained in previous investigations for pozzolana (Di Natale et al., 2006), Kaolin minerals (Yilmaz et al., 2017) and zeolite (Fang et al., 2018).

The Dubinin–Radushkevich (D-R) isotherm is used to differentiate between physical and chemical adsorption. Equation (6) describes the model (Chen, 2015).

$$Lnq_e = Ln(q_s) - \beta\varepsilon^2 \qquad (eq.6)$$

Where q_e denotes the equilibrium quantity of solute adsorbed per unit weight of solid (in mol. g^{-1}) and q_s denotes adsorbent uptake per unit weight (in mol.g^{-1}), β is the D–R isotherm constant (mol^2/kJ^2).(E, kJ/mol) is the mean adsorption energy (E) and ε is the Polanyi potential. The adsorption average free energy (E, kJ/mol) is calculated by (eq.7):

$$E = \left(\frac{1}{\sqrt{-2\beta}}\right) \qquad (eq.7)$$

Figure 9d and Table 2 displays also the Dubinin–Radushkevich constants resulting from the linear fitting of the experimental adsorption data. It has been established that adsorption is physical in nature if the mean adsorption energy E < 8 (kJ/mol) (Susmita and Krishna, 2014).

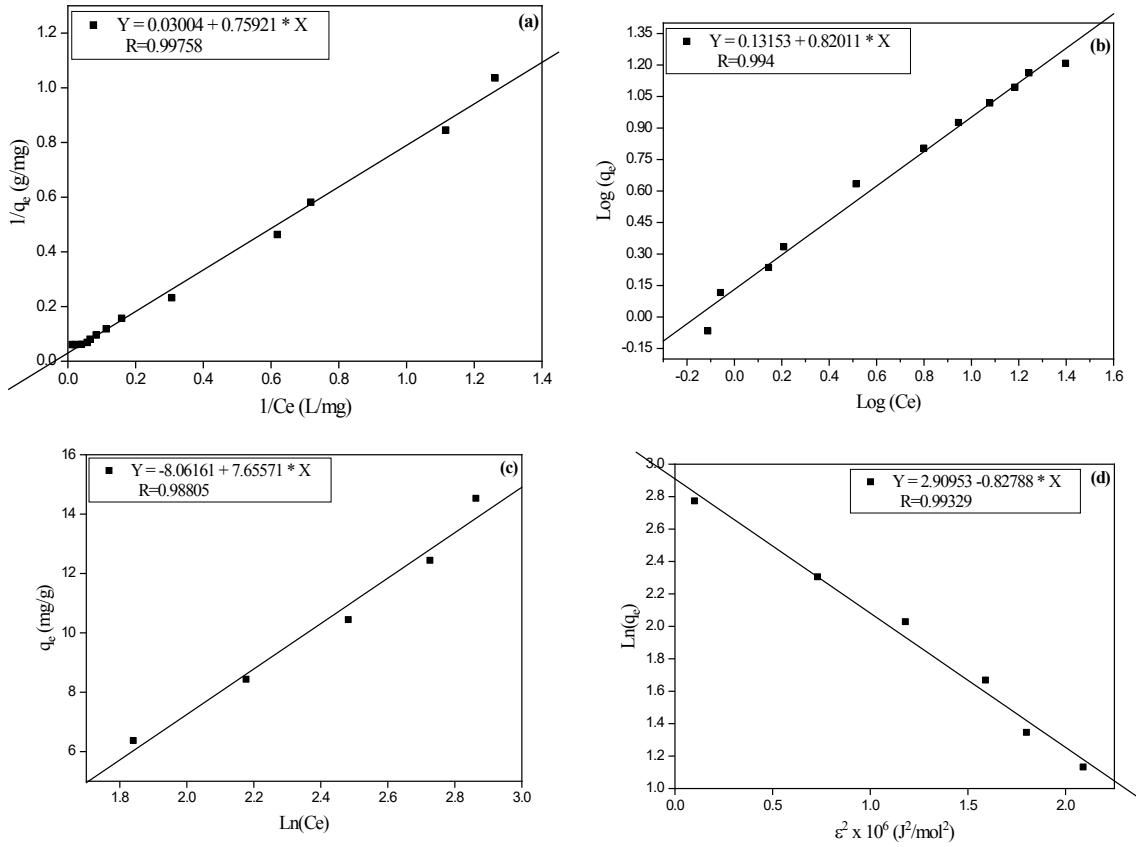

Fig. 9. Linear isotherm models of Hg(II) adsorption onto quartz surface: (**a**)Langmuir, (**b**)Freundlich, (**c**) Temkin and **(d)** Dubinin–Radushkevich (pH = 2 , T = 25°C and sorbent dose =1.0 g/L; [Hg(II)]=20-500 mg/L).

The calculated average adsorption free energy is 0.78 (kJ/mol), suggesting that physisorption is the prevailing adsorption mechanism for Hg(II) onto quartz mineral.

The effect of contact time on Hg(II) adsorption is given in Figure 10, the kinetics is characterized by a faster removal interval situated within 120 minutes, suggesting that Hg(II) metal ions increasingly occupied the negative adsorption sites on the quartz surface. The ionic diffusion generated by the stirring speed might be permitted to have rapid adsorption kinetics (Boudrahem et al., 2011). The adsorbed amount tends to stabilize and reaches equilibrium between 180 and 260 minutes. Within a contact time of 180 minutes, the maximum adsorption quantity of 16.31 mg/g was observed.

The adsorption kinetics was established by the pseudo-first-order model, pseudo second-order model and intra-particle diffusion (IPD) model following equations (8, 9 and 10) (Ho et al., 2000).

$$\frac{1}{q_t} = \frac{1}{q_e} + \left(\frac{K_1}{q_e}\right) \times \left(\frac{1}{t}\right) \qquad (eq.8)$$

$$\frac{1}{q_t} = \frac{1}{K_2 q_e^2} + \left(\frac{1}{q_e}\right) t \qquad (eq.9)$$

$$q_t = K_p t^{1/2} + C \qquad (eq.10)$$

Where q_e and q_t (mg/g) are the adsorption quantity at equilibrium and time t (min), respectively. K_1(1/min) and K_2 (g/mg.min) are the first and second-order rate constants, respectively. K_p is the intraparticle diffusion rate constant (g/mg.min$^{1/2}$), $t^{1/2}$ is a half-time adsorption equilibrium reaction, and C (mg/mg) is a constant. The kinetic rate constants K_1 and q_e (eq.3) were determined from the plots of $1/q_t$ against 1/t in. However, K_2 and q_e (eq.4) may be calculated by graphing t/q_t against t. A plot of q_t vs $t^{1/2}$ can be used to calculate the intraparticle diffusion rate K_p.

Figure 11 and Table 3 list the values of the rate kinetics constants, adsorption capacity $q_{e,cal}$, and the correlation coefficients (R^2). The linear treatment of the pseudo-first order adsorption kinetics of Hg(II) onto quartz surface is shown in Figure11a. The correlation coefficient R^2 is close to 0.998, but the relative error between the experimental ($q_{e,exp}$) and the estimated ($q_{e,cal}$)

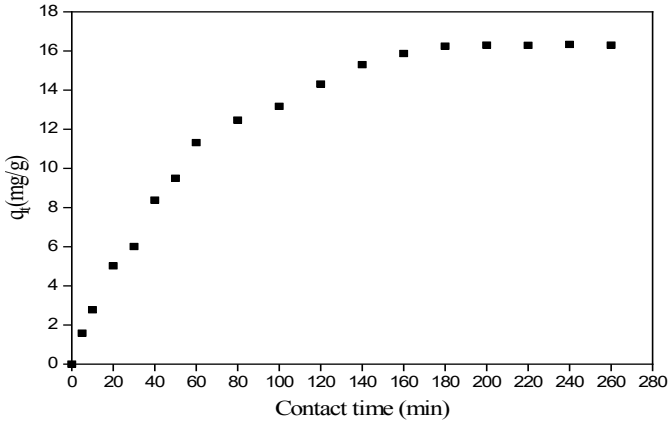

Fig. 10. The influence of contact time on the elimination of Hg(II) by quartz (Hg(II) = 500 mg/L,T=25 °C, pH = 2.0, adsorbent dose = 1.0 g/L and agitation speed = 200 rpm).

adsorption capacities is χ^2 =1.21. Figure 11b shows the linear plot of the pseudo-second-order kinetics model. The estimated relative error is χ^2 = 0.91 and the experimental adsorption capacity (q_{exp}) is better close to the calculated (q_{cal}) value. The correlation coefficient R^2 appears to be more than 0.99 (Table 3). The adsorption of Hg (II) ions by quartz mineral was most likely a second order process, according to the results. Similar results have been reported for Hg(II) adsorption on various adsorbent such as: Coal fly ash (Attari et al., 2017), L–Cysteine/LDHs (Bingbing et al., 2020), zeolite (Marin et al.,2020), hydroxyl apatite (Kim & Lee, 2014) and modified carbon (Al-Yaari and Saleh, 2022).The authors found that the pseudo-second-order kinetics model well described the adsorption data for mercuric ions adsorption.

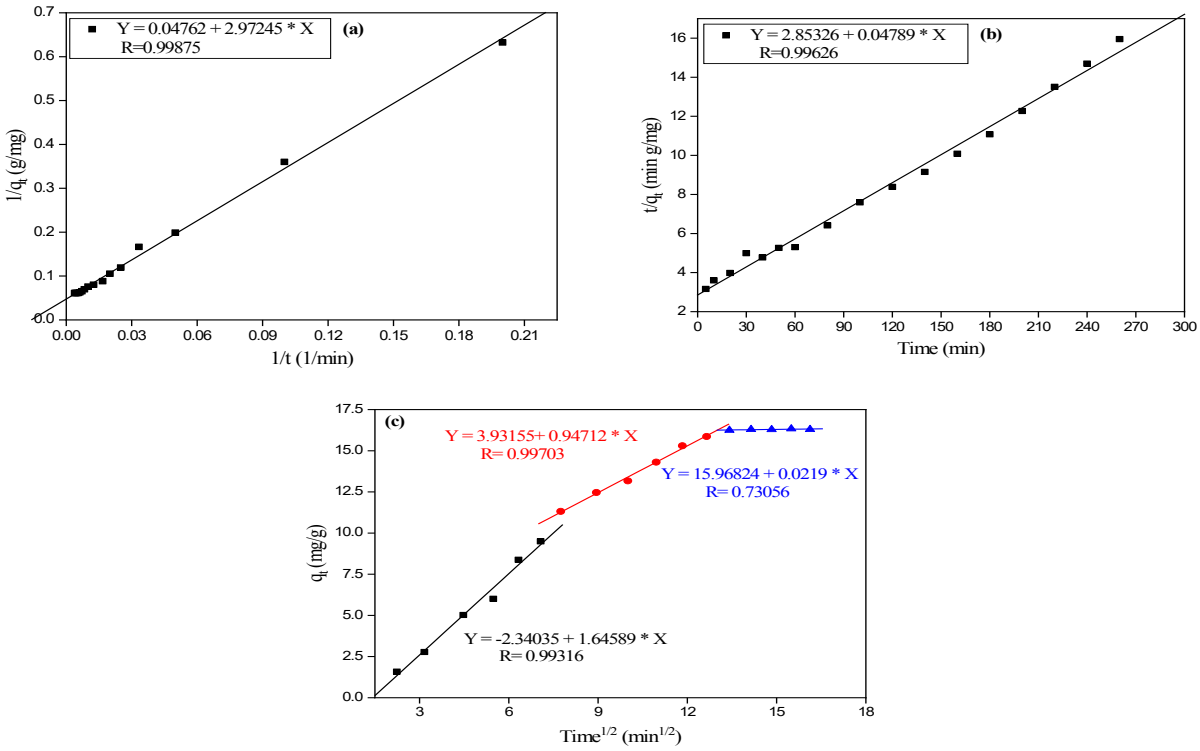

Fig. 11. Plots of the pseudo-first-order (**a**); pseudo-second-order kinetics (**b**) and intra-particle diffusion models (**c**) for Hg(II) adsorption onto quartz (T = 250°C and pH = 2.0).

Table 3. Kinetic parameters for Hg(II) adsorption onto quartz.

Pseudo-first-order model				**Pseudo-second-order model**			
K_1 (1/min)	$(q_{e,cal})$ (mg/g)	R^2	χ^2	K_2 (min.g/mg)	$(q_{e,cal})$ (mg/g)	R^2	χ^2
62.42	21.00	0.998	1.21	8.04×10^{-4}	20.88	0.993	0.91

Intra article diffusion model

Adsorption stage	K_p (mg/g.min$^{0.5}$)	C	R^2
Instantaneous	1.65	-2.34	0.986
Gradual	0.95	3.93	0.994
Equilibrium	0.022	15.97	0.534

$\chi^2 = (\Sigma(q_{e,exp} - q_{e,cal})^2 / q_{e,cal})$, $q_{e,exp}$ and $q_{e,cal}$ are the experimental and calculated amount adsorbed

Table 4. Comparison of the maximum adsorption capacity for Hg (II) on different inorganic adsorbents.

Adsorbent	pH	q_m (mg/g)	Ref
Coal fly ash	2.5	0.44	(Attari et al., 2017)
L–Cysteine/LDHs	5.0	215.90	(Bingbing et al., 2020)
Sulfur-modified zeolites	4.0	12.10	(Fang et al., 2018)
Pozzolana	6.5	0.80	(Di Natale et al., 2006)
MoS_4-LDH	2.6	11.0	(Ma et al., 2017)
Chitosan /Fe_3O_4	6.5	10.0	(Nasirimoghaddam et al., 2015)
ZSM-5 zeolite	7.0	51.54	(Rostami et al., 2018)
Bentonite	4.0	52.90	(Wang et al., 2011)
Magnetic Silica NC	-----	17.70	(Wang et al., 2018)
Kaolin minerals	7.4	30.10	(Yilmaz et al., 2017)
Modified pyrite (MPy)	3	54.44	(Yucheng et al., 2020)
Quartz	2.0	16.52	This work

The intra-particle diffusion (IPD) model is also used to analyze the diffusion mechanism. Figure 11c shows the plots of $q_{tr.}$ versus $t^{1/2}$ for the mercuric ions Hg(II). The values of the external diffusion constant K_{ip} and correlation coefficients R^2 are given in Table 3.

Figure 11c shows a multilinearity appearance, implying that three phases in the adsorption process are occurring. The values of the external diffusion constant K_p are very significant when considering the instantaneous 1.65 (mg/g.min$^{0.5}$) and gradual 0.95 (mg/g.min$^{0.5}$) adsorption stages. However, at the equilibrium stage it becomes of no consequence ($R^2 = 0.534$ and $K_p = 0.022$ (mg/g.min$^{0.5}$)). When comparing the values of Kp_1, kp_2 and kp_3. We found that they follow the rule $Kp_1 > kp_2 > Kp_3$ indicating an individual increases in the boundary layer on the adsorption stages (Labidi and Mechati, 2022). In the IPD model, the values of R^2 (< 0.995) were lower than in the pseudo-second-order (PSO) model. Hence, it was concluded that the intraparticle diffusion models cannot be applied as the limiting step, but other kinetic processes may be operating simultaneously (Bhatt et al., 2018; Al-Yaari and Saleh, 2022; Labidi and Mechati, 2022).

To assess quartz mineral as a prospective sorbent, the maximum adsorption capacity of Hg (II) is compared to that of other adsorbents published in the literature. According to Table 4, the natural quartz material used in this investigation exhibit a reasonable adsorption capacity of 16.51 mg/g for Hg (II) when compared with coal fly ash (0.44 mg/g) (Attari et al., 2017) and pyrite (54.44 mg/g) (Yucheng et al., 2020). The mercuric removal capacity of quartz mineral is approximately 38 times higher than that of coal fly ash and 21 times than that in pozzolana (Di Natale et al., 2006). However, a ratio of 0.30 is observed for pyrite. The quartz mineral engaged in this investigation has a satisfactory adsorption potential as compared to other reported natural material. Also, because of the natural character and geological abundance in Algeria, the quartz mineral used in this study is cheap and presents an economic advantage as low-cost adsorbent.

CONCLUSIONS

The quartz mineral used in this adsorption experiments includes 99.13% SiO_2 and has a surface area of 0.6 (m^2/g). According to zeta potential measurements, the quartz mineral had an isoelectric point (I.E.P.) at pH = 1.8. Quartz mineral showed a good adsorption capacity to Hg(II) ions in aqueous solution, the highest experimental uptake is 16.52 (mg/g) at 180 min. Based on Langmuir and pseudo second-order adsorption models, it was confirmed that the Hg(II) adsorption process was a mono-layered adsorption controlled by physical adsorption. The intra-particle diffusion model shows an adsorption process within three stages. The calculated Dubinin–Radushkevich mean sorption energy of 0.78 (kJ/mol), indicates that the sorption is physical in nature.

This work opens an intresting perspective in the field of heavy metal removal from wastewater with natural and low cost sorbents. Work is in progress to study: (i) the effect of experimental parameters affecting the adsorption process such as agitation speed, quartz particles seize and temperature. (ii) Regeneration study and (iii) The mechanism of Hg(II) elimination considering the thermodynamic, spectroscopic (DRX and FTIR) and theoretical semi-empirical calculations.

GRANT SUPPORT DETAILS

The present research did not receive any financial support.

CONFLICT OF INTEREST

The authors declare that there is no conflict of interests regarding the publication of this manuscript.

LIFE SCIENCE REPORTING

No life science threat was practiced in this research.

REFERENCES

Al-Yaari, M. and Saleh T.A. (2022). Mercury removal from water using a novel composite of polyacrylate-modified carbon. ACS Omega., 7, 14820-14831.

Al-Ghouti, M.A., Da'ana, D., Abu-Dieyeh, M. and Majeda, K. (2019). Adsorptive removal of mercury from water by adsorbents derived from date pits. Sci Rep., 9, 15327.

Attari, M., Bukhari, S., Kazemian, H. and Rohani, S. (2017). A low-cost adsorbent from coal fly ash for mercury removal from industrial wastewater. J. Environ. Chem. Eng., 5, 391– 399.

Babic, B.M., Milonjic, S.K., Polovina, M.J., Cupic, S. and Kaludjerovic, B.V. (2002). Adsorption of zinc, cadmium and mercury ions from aqueous solutions on an activated carbon cloth. Carbon., 40, 1109–1115.

Bhatt, R., Kushwaha, S., Bojja, S. and Padmaja, P. (2018). Chitosan thiobarbituric acid: A super adsorbent for mercury. ACS Omega., 3(10),13183–13194.

Boudrahem, F., Aissani-Benissad, F. and Soualah A. (2011). Adsorption of lead (II) from aqueous solution by using leaves of date trees as an adsorbent. J. Chem. Eng. Data, 56, 1804–1812.

Bingbing, L., Meng, C., Feifei, C. and Zhiyong, X. (2020). L–Cysteine/hydrotalcite hybrid for collaborative removal of Cu(II), Hg(II) and Pb(II) ions from aqueous solutions: different metal ions require different mechanisms. Chemistry Select., 5(16), 4932– 4942.

Chen, X. (2015). Modeling of experimental adsorption isotherm data. Information., 6, 14–22.

Di Natale, F., Lancia, A., Molino, A., DiNatale, M., Karatza, D. and Musmarra, D. (2006). Capture of mercury ions by natural and industrial materials.J. Hazard. Mater B., 132, 220– 225.

Fang, R.Y., Lu, C.W.; Zhang, W.K., Xiao, Z.; Chen, H.F., Liang, C., Huang, H., Gan, Y.P., Zhang, J. and Xia, Y. (2018). Supercritical CO_2 assisted synthesis of sulfur-modified zeolites as high-efficiency adsorbents for Hg^{2+} removal from water. New. J. Chem., 42, 3541–3550.

Hadi, P., To, M.H., Hui, C.W., Carol, S.K.L and McKay, G. (2015). Aqueous mercury desorption By activated carbons. Water Res., 73, 37–55.

Ho, Y.S., Ng, J.C.Y. and McKay, G. (2000). Kinetics of pollutant sorption by biosorbents. Review. Sep. Purif. Rev., 29(2), 189-232.

Hui, W., Haotian, S., Chang, S., Yaning, L., Zhanfeng, Y. and Yufeng, D. (2019). Kinetics and mechanism study of mercury adsorption by activated carbon in wet oxy-fuel conditions. Energy Fuels., 33(2), 1344–1353.

Jianjian, Z., Liping, L., Ziwei, L., Zhaofeng, D., Yufeng, L., Subin., Zhongxin,X., Wenlong, X. and Yuzhong, N. (2020).The adsorption property and mechanism for Hg(II) and Ag(I) by schiff base functionalized magnetic Fe_3O_4 from aqueous solution. J. Alloys and Compd., 825, 154051.

Kang, H., Xueliu, X., Zhiping, L., Dong, F., Rui, B. and Jianhong, Yi. (2020). Effective removal of mercury Ions in aqueous solutions: A Review. Curr. Nanosci., 16 (3), 363–375.

Kosak, A., Lobnik, A. and Bauman, M. (2015). Adsorption of mercury (II), lead(II), cadmium(II) and

zinc(II) from aqueous solutions using mercapto-modified silica particles. Int. J. Appl. Ceram Technol., 12(2), 461– 472.
Kim, Y. and Lee, Y.J. (2014). Characterization of mercury sorption on hydroxylapatite: batch studies and microscopic evidence for adsorption. J Colloid Interface Sci., 430, 193–199.
Labidi, N.S. and Mechati, B. (2022). Adsorption mechanism of basic blue-9 onto quartz mineral: kinetics, isotherms and thermodynamic. Mater. Res. Express., 9, 115501.
Levien, L., Prewitt, C.T. and Weidner, D.J. (1980). Structure and elastic properties of quartz at pressure P = 1 atm. Am Min., 65, 920–930.
Liangyan, D., Xiude, H., Deshuai, S., Yongzhuo, L., Qingjie, G., Tongkai, Z. and Botao, Z. (2020). Rapid removal of low concentrations of mercury from wastewater using coal gasification slag. Korean J Chem Eng., 37(7), 1166-1173.
Liuwei, W., Deyi, H., Yining, C., Yong, S.O., Filip, M.G. T., Jörg, R. and O'Connor, D. (2020). Remediation of mercury contaminated soil, water, and air: A review of emerging materials and innovative technologies. Enviro. Int., 134, 105281.
Ma, L., Islam, S.M., Xiao, C., Zhao, J., Liu, H., Yuan, M., Sun, G., Li, H., Ma, S. and Kanatzidis, M.G. (2017). Rapid simultaneous removal of toxic anions $[HSeO_3]^-$, $[SeO_3]^{2-}$, and $[SeO_4]^{2-}$, and metals Hg^{2+}, Cu^{2+}, and Cd^{2+} by MoS_4^- intercalated layered double hydroxide. J. Am. Chem. Soc., 139(36), 12745-12757.
Marin, U., Teja, C., Ivona, N. and Marina, T. (2020). Comparative study of mercury (II) removal from aqueous solutions onto natural and iron-modified clinoptilolite rich zeolite. Processes., 8(11), 1523.
Nadhira, I.S., Fidela, A.A., Della, A., Ridha, D.R., Ilham, S. and Sri, W. (2018). NPK Fertilizer with slow-release fly ash. J. Pure App. Chem. Res., 7(1), 1-11.
Nasirimoghaddam, S., Zeinali, S. and Sabbaghi, S. (2015). Chitosan coated magnetic nano-particles as nano-adsorbent for efficient removal of mercury contents from industrial aqueous and oily samples. J. Ind. Eng. Chem., 27, 79–87.
Olugbenga, S. B., Kayode A.A. and Rhoda, O.O. (2014).Insights into the adsorption of heavy metals from wastewater using diatomaceous earth. Sep. Sci. Technol., 49, 1787–1806.
Powell, K.J., Brown, P.L., Byrne, R.H., Gajda, T., Hefter, G., Sjöberg, S. and Wanner, H. (2005). Chemical speciation of environmentally significant heavy metals with inorganic ligands part 1: The Hg^{2+}– Cl^-, OH^-, CO_3^{2-}, SO_4^{2-}, and PO_4^{3-} aqueous systems. Pure Appl.Chem., 77(4), 739-800.
Purohit, P., Somasundaran, P. and Kulkarni, R. (2006). Study of properties of modified silicones at solid–liquid interface: Fabric–silicone interactions. J. Colloid Interface Sci., 298, 987-990.
Rostami, S., Azizi, S.N. and Asemi, N. (2018). Removal of mercury (II) from aqueous solutions via Box-Behnken experimental design by synthesized hierarchical nanoporous ZSM-5 zeolite. J. Iran Chem. Soc., 15, 1741-1754.
Saikia, B.J., Parthasarathy, G. and Sarmah, N.C. (2008).Fourier transform infrared spectroscopic estimation of crystallinity in SiO_2 based rocks. Bull. Mater. Sci., 31(5), 775-779.
Sears, G. (1956). Determination of specific surface area of colloidal silica by titration with sodium hydroxide. Anal. Chem., 28(12), 1981-1983.
Susmita, S.G. and Krishna G.B. (2014). Adsorption of metal ions by clays and inorganic solids. RSC Advances., 4(54), 28537-28586.
Tabrizy, V.A., Hamouda, A.A. and Denoyel, R. (2011). Influence of magnesium and sulfate ions on wettability alteration of calcite, quartz, and kaolinite: Surface energy analysis. Energy & Fuels., 25(4), 1667-1680.
Tuzen, M., Sari, A., Mendil, D. and Soylak, M. (2009).Biosorptive removal of mercury (II) from aqueous solution using lichen (Xanthoparmelia conspersa) biomass: kinetic and equilibrium studies. J. Hazard. Mater., 169(1–3), 263–270.
Volesky, B. (1994). Advances in biosorption of metals: selection of biomass types. FEMS Microbiol Rev., 14(4), 291–302.
Wang, Q.H., Chang, X. J., Li, D.D., Hu, Z., Li, R. J. and He, Q. (2011). Adsorption of chromium(III), mercury(II) and lead(II) ions onto 4-aminoantipyrine immobilized bentonite. J. Hazard. Mater., 186(2-3), 1076-1081.
Wang, Y.Y., Tang, M.Y., Shen, H., Che, G.B., Qiao, Y., Liu, B. and Wang, L. (2018). Recyclable multifunctional magnetic mesoporous silica nanocomposite for ratiometric detection, rapid adsorption and efficient removal of Hg (II). ACS Sustain.Chem.Eng., 6, 1744-1752.
Yilmaz, S., Sahan, T. and Karabakan, A. (2017). Response surface approach for optimization of Hg (II) adsorption by 3-mercaptopropyl trimethoxysilane-modified kaolin minerals from aqueous solution. Korean J. Chem. Eng., 34, 2225-2235.
Yucheng, Z., Shuchuan, P., Ping L., Tianhu, C. and Yan, Y. (2020). Mercury removal from aqueous solutions using modified pyrite: A Column Experiment. Minerals., 10(1), 43.